Analyst

PAPER

View Article Online
View Journal

Cite this: DOI: 10.1039/d6an00156d

Design of a "turn-on" colorimetric sensor for AChE inhibitors based on the instability of metal–organic frameworks

Jun Zhang, Wenzhu Jiang, Zhiping Xu and Lin Zhang *

Received 8th February 2026,
Accepted 30th March 2026

DOI: 10.1039/d6an00156d

rsc.li/analyst

Generally, unstable metal–organic frameworks (MOFs) have been less commonly employed in many applications compared to stable MOFs. However, given the vast number of such unstable MOFs and the diversity of their instability behaviors, exploring their effective utilization is both necessary and significant. Unlike previous reports, this work mainly focused on the specific instability of Cu-BTC towards thiocholine, which was generated through the enzymatic hydrolysis of acetylthiocholine chloride (ATCl) by acetylcholinesterase (AChE). In detail, Cu-BTC exhibited outstanding peroxidase-like activity, efficiently catalyzing the oxidation of 3,3′,5,5′-tetramethylbenzidine (TMB) into its oxidized form, generating a strong UV–vis absorption peak at 655 nm. Upon the addition of AChE and its substrate ATCl, the substrate was hydrolyzed by AChE to yield thiocholine (TCl), which triggered the disintegration of Cu-BTC, thereby inhibiting TMB oxidation. As expected, based on the thiocholine-induced disintegration of Cu-BTC, the sensor enabled the selective and sensitive visual detection of the AChE inhibitor chlorpyrifos with a low detection limit of 8.95 pM. This method was successfully applied to pesticide analysis in spiked vegetable samples, achieving recoveries ranging from 98.83% to 109.81% with relative standard deviations below 2.57%. The proposed strategy not only provides a simple and visual approach for food safety monitoring but also opens new possibilities for exploiting unstable MOFs as smart sensing platforms.

1. Introduction

Organophosphorus pesticides (OPs) are highly effective insecticides and are of great importance in agricultural production.[1–3] However, the overuse of OPs poses substantial risks to environmental and food safety, leading to pesticide residues in crops and impairment of ecosystem functions.[4,5] The primary mechanism of OP toxicity is the irreversible inhibition of acetylcholinesterase (AChE), which results in the systemic accumulation of acetylcholine and sustained cholinergic overstimulation, potentially causing diverse pathological conditions such as cancer, neurological disorders, and reproductive system diseases.[6,7] Critically, OPs exhibit bioaccumulative potential across trophic levels, resulting in increased accumulation in organisms along the food chain and causing persistent ecologically significant harm.[8,9] Consequently, there is an urgent need for robust, broadly applicable, and operationally efficient methods to detect AChE inhibitors with high sensitivity and specificity. Various analytical methods have been proposed for detecting AChE activity and its inhibitors, including colorimetry, fluorescence, electrochemical methods; TLC-direct bioautography; and chemiluminescence.[10–16] Among these, colorimetric detection has garnered particular attention due to its visual accessibility, high precision, and ease of operation, as it relies on the quantitative or comparative measurement of the absorbance generated by colored reaction products.[17,18] Considering the significant impact of AChE on human health, there is an urgent need to develop a simple, nontoxic, economical, and label-free colorimetric system for the real-time monitoring of AChE activity and the high-throughput screening of its inhibitors.

Recently, metal–organic frameworks (MOFs), a type of crystalline porous materials composed of metal ions or clusters and polytopic organic ligands, have garnered significant attention across various fields, including separation, gas adsorption, energy storage, catalysis, sensing, and drug delivery.[19–23] Benefiting from their abundant conjugated systems and binding sites, MOFs have emerged as promising platforms for chemical sensing. In these studies, MOFs with excellent chemical and structural stability were preferentially selected.[24–29] However, it cannot be ignored that a considerable proportion of reported MOFs possess intrinsic instability. Notably, these materials can display distinct environmental sensitivity, particularly toward small molecules and ions.[30–35] For example, ZIF-90 has been shown to respond selectively to ATP, exhibiting ATP-induced disintegration.[36,37] Similarly, the

Shenyang Key Laboratory of Medical Molecular Theranostic Probes in School of Pharmacy, Shenyang Medical College, Shenyang 110034, China.
E-mail: zl210503@163.com

crystals of ZIF-8 are susceptible to degradation in aqueous solutions containing divalent and trivalent metal ions.[38] Undoubtedly, to fully exploit the distinctive features of MOFs, systematically exploring the stimulus-responsive behavior of unstable MOFs will be of great importance and necessity. Although MOF instability is typically regarded as a drawback and its use is avoided in many applications, this inherent limitation may be transformed into an advantage in certain applications.

Significant progress has been made in developing nanozyme-based sensors for the detection of AChE inhibitors, with materials such as Fe–N–C single-atom catalysts and robust COF-based composites being prime examples.[39,40] These systems typically rely on their stable, enzyme-like activities to generate detectable signals upon the introduction of inhibitors. Although effective, their design strategy primarily focuses on maintaining structural integrity. In this work, we propose that the controlled disintegration of an unstable MOF, triggered by a specific enzymatic reaction product, can serve as the basis for a highly sensitive biosensing platform. To test this hypothesis, we selected Cu-BTC, a MOF with intrinsic peroxidase-like enzymatic activity, as our model system. It is known that Cu-BTC is unstable towards S-containing molecules such as thiocholine (TCl), which is generated *via* the AChE-catalyzed hydrolysis of acetylthiocholine chloride (ATCl).[41–43]

Building on this principle, we developed a colorimetric platform for AChE inhibitor detection. In the absence of inhibitors, AChE hydrolyzed ATCl to produce TCl, which triggered Cu-BTC disintegration, preventing TMB oxidation. Conversely, in the presence of OPs, AChE activity was inhibited, resulting in a reduced generation of TCl. Under these conditions, the Cu-BTC framework remained structurally intact, enabling the efficient oxidation of TMB to yield a pronounced blue color with a characteristic absorption peak at 652 nm. The proposed system could sensitively and selectively detect the AChE inhibitor chlorpyrifos with a detection limit of 8.95 pM, which is substantially lower than those of previously reported sensing systems. This work highlights a unique conceptual contribution, which resides in its use of MOF instability as an intrinsic signal transduction mechanism, despite this property being commonly regarded as a fundamental limitation. More broadly, this study not only provides an efficient strategy to construct sensors for thiol-containing analytes but also offers a facile approach to utilize the instability of MOFs.

2. Experimental section

2.1. Materials and instruments

Acetylcholinesterase (AChE, 500 U mg^{-1}), acetylthiocholine chloride (ATCl), 3,3′,5,5′-tetramethylbenzidine (TMB), benzene-1,3,5-tricarboxylic acid (H_3BTC), and $Cu(NO_3)_2$ were obtained from Shanghai Macklin Biochemical Technology (Shanghai, China). Potassium chloride (KCl), *N*,*N*-dimethylformamide (DMF), hydrogen peroxide (H_2O_2), acetic acid (HAc), sodium acetate (NaAc), ethanol, chlorpyrifos, emamectin benzoate, triadimefon and deltamethrin were obtained from Aladdin Industrial Co., Ltd (Shanghai, China). All chemical reagents were of analytical grade and used as received without further purification. 0.1 M sodium acetate buffer (NaAc–HAc, pH 4.5) was used as the working buffer in all experiments. Doubly distilled water was employed throughout the study.

The morphology of the as-prepared sample was characterized using scanning electron microscopy (SEM, Carl Zeiss Microscopy GmbH, Germany). Powder X-ray diffraction (PXRD) patterns were collected on a German Bruker D8 Advance X-ray powder diffractometer using Cu Kα radiation (λ = 1.5418 Å). Fourier transform infrared (FT-IR) spectra were recorded in the range of 4000–500 cm^{-1} with KBr pellets on a Bruker Vertex 70 FI-IR spectrophotometer (Germany). Absorbance measurements were performed using a UV–vis spectrophotometer (T6 New Century, Puxi, China).

2.2. Synthesis of Cu-BTC

Cu-BTC was synthesized *via* a hydrothermal route following a modified literature procedure.[37] Briefly, 1.0 g of 1,3,5-benzenetricarboxylic acid (H_3BTC) was dissolved in a mixture of DMF and ethanol (15 mL each), followed by the addition of an aqueous solution of $Cu(NO_3)_2$ (0.57 mol L^{-1}, 15 mL) under vigorous stirring. The resulting mixture was transferred to a Teflon-lined stainless steel autoclave and heated at 373 K for 10 h. After cooling to room temperature, the precipitate was collected by centrifugation and subsequently washed three times with DMF, deionized water, and ethanol to afford the final Cu-BTC product.

2.3. Evaluation of the peroxidase-like activity

The peroxidase-like activity of Cu-BTC was confirmed through the direct catalytic oxidation of TMB in the presence of H_2O_2. A reaction mixture was prepared by combining 2 mL of NaAc–HAc buffer (pH 4.5), 50 μL of Cu-BTC (1 mg mL^{-1}), 10 μL of H_2O_2 (2.0 mM), and 50 μL of TMB (10.0 mM). Following incubation at 37 °C for 25 min, the colorimetric change was visually observed, and the absorbance of the oxidized product (oxTMB) was measured at 652 nm using a UV–vis spectrophotometer to record the peroxidase activity.

2.4. Optimization of the detection conditions

The peroxidase-like activity of Cu-BTC was systematically optimized by investigating the effects of Cu-BTC concentration, pH, reaction time, and temperature. All experiments were performed based on a typical chromogenic reaction, using TMB as the substrate in the presence of H_2O_2. The catalytic reaction conditions of the Cu-BTC were optimized *via* a single-factor method. The effects of Cu-BTC concentration (0.2–1.4 mg mL^{-1}), buffer pH (3.0–5.5), reaction time (5–30 min) and reaction temperature (4–50 °C) were investigated. The absorbance at 652 nm was used to determine the optimal reaction parameters. All measurements were performed in triplicate, and the optimized conditions were subsequently applied to the chlorpyrifos detection assay.

2.5. Detection of the AChE inhibitor

For the colorimetric assay, 50 μL of AChE (0.5 U μL^{-1}) was mixed with 20 μL of chlorpyrifos at various concentrations in 2.0 mL of 0.1 M NaAc–HAc buffer (pH 4.5), followed by incubation at 37 °C for 10 min. Subsequently, 60 μL of ATCl solution (8 mM) was added, and the mixture was incubated at room temperature for 20 min. After that, 0.5 mL of Cu-BTC (1.0 mg mL^{-1}) was introduced and allowed to react for 30 min. After centrifugation, the supernatant was collected, and 10 μL of H_2O_2 (2.0 mM), 50 μL TMB (10.0 mM) and 2 mL of NaAc–HAc buffer (pH 4.5) were added. A color change was observed, and the UV–vis absorption spectrum was recorded after 25 min at a wavelength of 652 nm. The inhibition rate of chlorpyrifos was calculated as follows:

$$\text{Inhibition } (\%) = [(A_1 - A)/(A_0 - A)] \times 100\%,$$

where A and A_1 are the absorbance values of the biosensor incubated without or with chlorpyrifos, respectively, and A_0 is the absorbance value in the absence of AChE.

2.6. Real sample analysis

To evaluate the practical applicability of the proposed strategy for pesticide detection in real samples, apples purchased from a local supermarket were selected as a representative fruit. The edible parts of apples were chopped and then homogenized. Subsequently, 30 mL of methanol was added to 3.0 g of the samples, and the mixture was stirred for 8 h, followed by centrifugation at 12 000 rpm for 30 min. The clear supernatant was collected and spiked with chlorpyrifos at concentrations of 100, 500, 5000, 100 000 and 1 000 000 pM. Finally, the spiked samples were analyzed using the proposed method, and each measurement was performed in triplicate.

3. Results and discussion

3.1. Principle of the colorimetric detection system of AChE inhibitors

A simple and reliable colorimetric platform for the quantitative detection of AChE inhibitors was developed by integrating the peroxidase-like activity of Cu-BTC and its specific instability towards thiocholine (Scheme 1). Cu-BTC exhibited outstanding peroxidase-like activity by catalyzing the oxidation of TMB into its blue-colored oxTMB product *via* hydroxyl radical (•OH) generation, yielding a strong UV–vis absorption peak at 652 nm. Upon the addition of AChE and ATCl, ATCl was hydrolyzed by AChE to yield thiocholine (TCl), which triggered the disintegration of Cu-BTC and consequently a loss of peroxidase-like activity. However, in the presence of an AChE inhibitor such as chlorpyrifos, AChE activity was suppressed, resulting in reduced TCl production and preservation of Cu-BTC integrity, thereby increasing the absorbance signal at 652 nm. Structural evidence supporting this mechanism is provided in Fig. S1. After exposure to ATCl/AChE reaction products, the characteristic peaks significantly diminished in intensity, with several peaks disappearing completely (Fig. S1a). SEM images further demonstrated morphological degradation, consistent with the structural disintegration (Fig. S1b). These results directly confirmed the TCl-induced collapse of Cu-BTC. Accordingly, this assay is based on a signal-amplified "turn-on" principle, enabling the sensitive and selective quantification of AChE inhibitors.

3.2. Characterization of the synthesized Cu-BTC

Cu-BTC was synthesized *via* a solvothermal reaction between $Cu(NO_3)_2$ and H_3BTC dissolved in DMF. As shown by the XRD analysis in Fig. 1a, all observed diffraction peaks matched well with the simulated pattern of Cu-BTC, confirming the success-

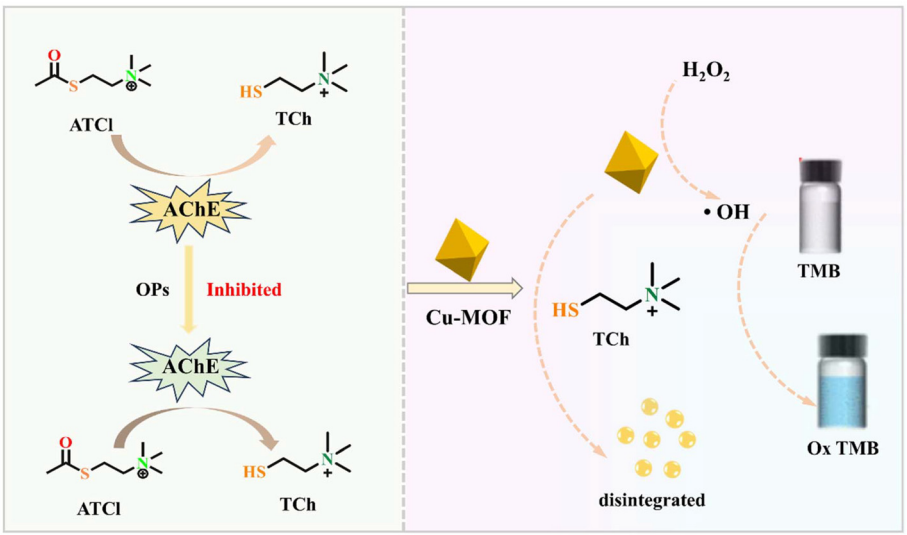

Scheme 1 Illustration of the colorimetric assay based on Cu-BTC with peroxidase-like activity for the AChE inhibitor.

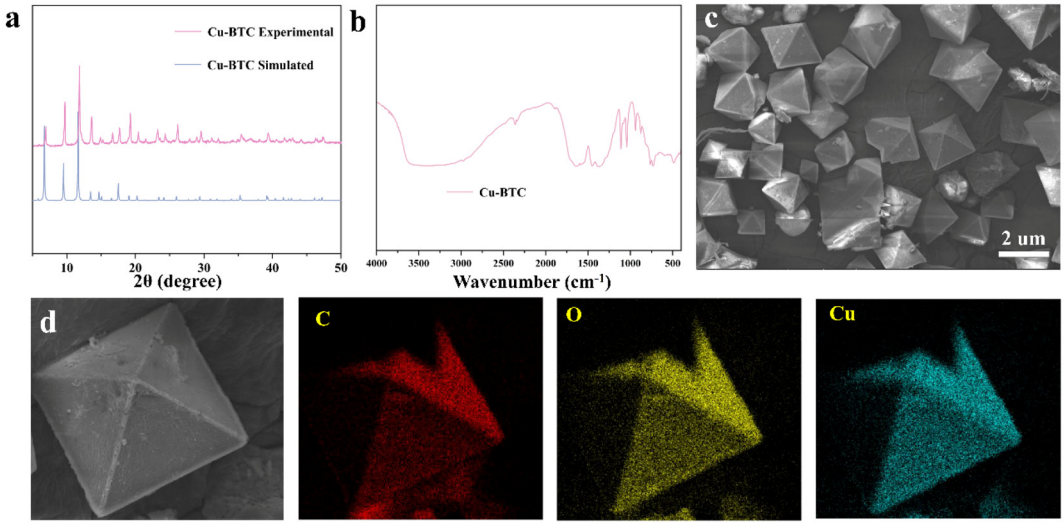

Fig. 1 (a) PXRD patterns, (b) FT-IR spectrum, (c) SEM image, and (d) EDS elemental mapping images of Cu-BTC.

ful formation of the expected framework structure. The chemical structure of the obtained MOF was further verified by FT-IR spectroscopy. The spectrum exhibited the characteristic vibrational bands associated with the Cu-BTC framework, confirming the presence of the organic linker and its coordination to the metal centers (Fig. 1b). SEM was used to examine the morphology of Cu-BTC, revealing a uniform and monodisperse structure with an average diameter of approximately 2 μm (Fig. 1c). Furthermore, energy-dispersive X-ray spectroscopy (EDS) mapping (Fig. 1d) confirmed that the elements Cu, O, and C were homogeneously distributed within the obtained MOF, indicating a well-constructed and chemically homogeneous material. In summary, these complementary characterizations provided robust evidence for the successful synthesis of phase-pure Cu-BTC with a uniform morphology, laying a solid foundation for subsequent sensing studies.

3.3. Peroxidase-like activity of Cu-BTC

To validate the peroxidase-like activity of Cu-BTC, TMB was employed as a chromogenic substrate to establish a colorimetric detection platform monitored by UV–vis spectroscopy. As shown in Fig. 2a, only the Cu-BTC system containing both H_2O_2 and TMB exhibited a distinct dark blue color after 25 min, with an absorbance intensity of 1.1 in the ultraviolet-visible absorption spectra. In contrast, negligible absorbance was observed in the control systems lacking either H_2O_2 or TMB, confirming that catalytic oxidation proceeded exclusively in the presence of both the oxidant and the substrate, thereby establishing a low intrinsic background. In addition, as shown in Fig. 2b, Cu-BTC retained 92.92% of its initial activity after 15 days, highlighting its excellent stability and potential for prolonged catalytic applications. To identify the active intermediates involved in the catalysis, electron paramagnetic resonance (EPR) spectroscopy was performed using 5,5-dimethyl-1-pyrroline *N*-oxide (DMPO) as a spin-trapping agent. In Fig. 2c, the 1 : 2 : 2 : 1 four-fold characteristic EPR signals assigned to the DMPO/˙OH adduct were detected in the Cu-BTC + DMPO + H_2O_2 system. These results confirmed that the peroxidase-like activity of Cu-BTC originated from a Fenton-like catalytic mechanism driven by the redox cycling of copper species. The coordinatively unsaturated metal sites within the Cu-BTC framework served as active centers for H_2O_2 activation. As extensively documented in the literature,[44] the generally accepted mechanism involves the reduction of the framework

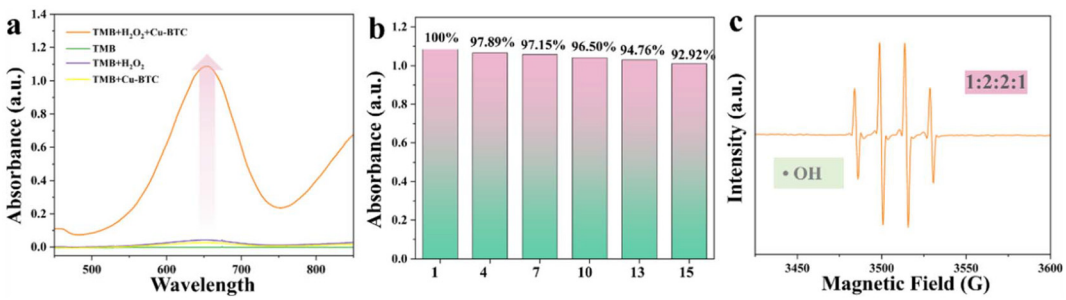

Fig. 2 (a) UV–visible absorption spectra of different solutions. (b) Storage stability of the developed biosensor over a period of 15 days. (c) ESR spectra of Cu-BTC.

Cu(II) to Cu(I) by H_2O_2, followed by the reaction of the generated Cu(I) with another H_2O_2 molecule to produce highly oxidative hydroxyl radicals ($^{\bullet}OH$). These $^{\bullet}OH$ radicals were subsequently responsible for the rapid oxidation of the chromogenic substrate TMB, thereby endowing the material with its peroxidase-mimicking activity.

3.4. Optimization of the experimental conditions

Prior to chlorpyrifos detection, the peroxidase-like activity of Cu-BTC was systematically optimized by varying several experimental parameters, including Cu-BTC concentration, pH, temperature, and reaction time. As illustrated in Fig. 3a, the absorbance at 652 nm increased progressively with Cu-BTC concentration and plateaued at 1.0 mg mL^{-1}. As a result, 1.0 mg mL^{-1} Cu-BTC was selected for the following experiments. Additionally, given the pH-dependent nature of peroxidase-like nanozymes, the pH of the NaAc–HAc buffer was also optimized across the range of 3.5–6.0 (Fig. 3b). At pH 4.5, the catalytic activity of Cu-BTC was the highest, suggesting that pH 4.5 is the optimal protonation environment for Cu-BTC-mediated TMB oxidation. Fig. 3c showed that the absorbance signal increased rapidly during the initial 20 minutes and reached equilibrium after 25 minutes, therefore a 25-minute reaction time was employed for all subsequent assays. Temperature dependence was assessed over the range of 25–45 °C, revealing a consistent increase in the peroxidase-mimicking activity with rising temperature. Since sufficient activity was achieved at 37 °C, subsequent experiments were conducted under these conditions. Hence, for optimal performance, chlorpyrifos detection experiments were conducted under the conditions of 1.0 mg mL^{-1} Cu-BTC at 37 °C, pH 4.5 and with a reaction time of 25 min.

3.5. Visual detection of the AChE inhibitor

Based on the remarkable peroxidase-like activity of Cu-BTC and its documented instability toward thiocholine, we developed a colorimetric sensing platform for the detection of the AChE inhibitor. The detection principle is schematically depicted in Scheme 1. The sensitivity of the proposed platform was evaluated by monitoring the absorbance response to varying concentrations of chlorpyrifos under the previously optimized conditions. As shown in Fig. 4a, the absorbance at 652 nm increased progressively with increasing chlorpyrifos concentration. A linear relationship was established between the absorbance intensity and the logarithm of the chlorpyrifos concentration over the range of 10^{-4}–10^{-11} M, yielding a linear regression equation of $y = 11.382x + 33.311$ with a coefficient of determination (R^2) of 0.995 (Fig. 4b). The limit of detection (LOD) was determined to be 8.95 pM based on a 10% inhibition. Moreover, the concentrations of the inhibitor correlated

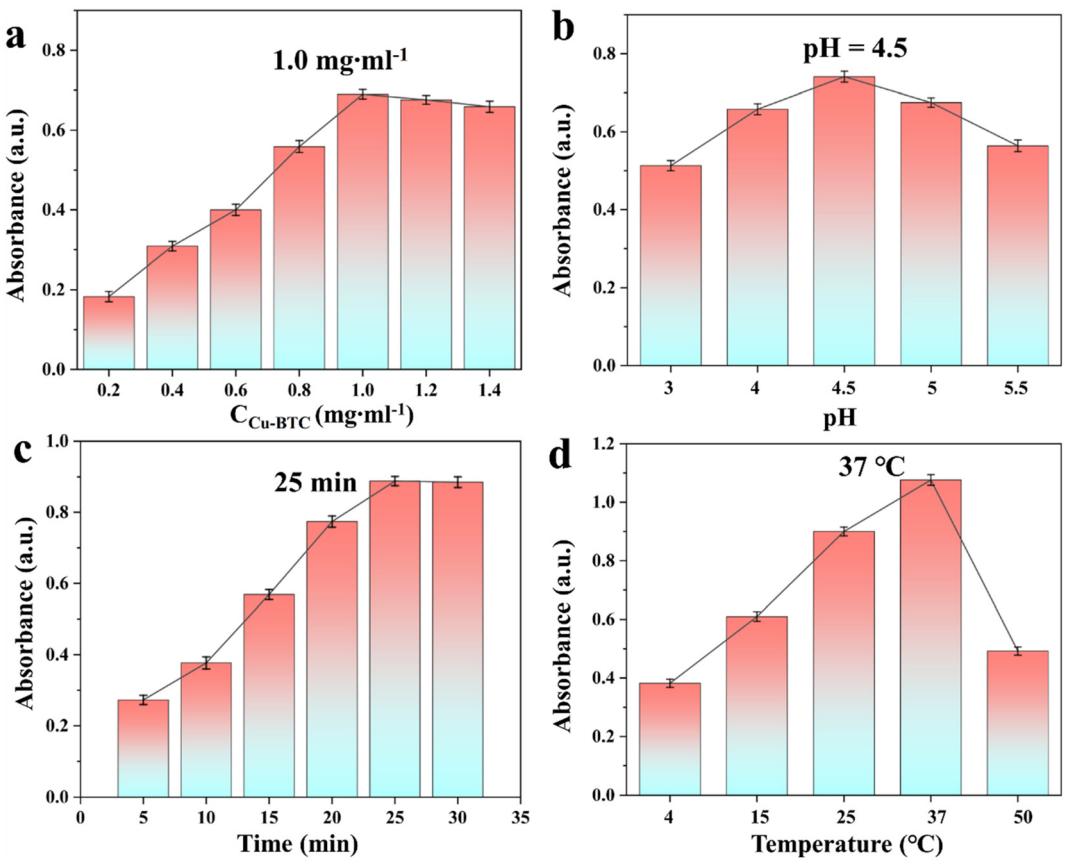

Fig. 3 Effects of (a) Cu-BTC concentration, (b) pH, (c)reaction time, and (d) temperature on the peroxidase activity of Cu-BTC.

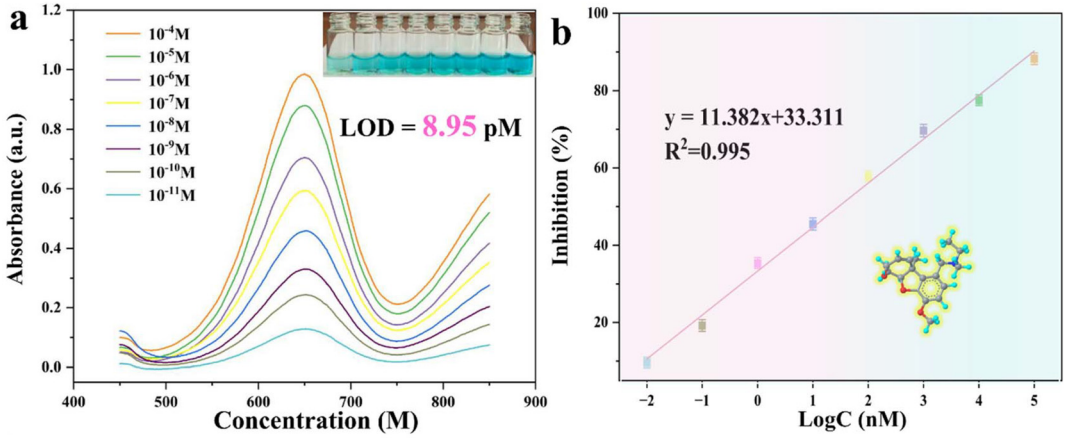

Fig. 4 (a) UV–visible absorbance spectra of the sensing system after incubation with different concentrations of chlorpyrifos for 20 min. (b) Corresponding calibration curve of the inhibition rate *versus* the logarithm of chlorpyrifos concentration.

directly with the observed color change. The color of oxTMB increased progressively with chlorpyrifos concentration, enabling reliable naked-eye discrimination across the quantifiable range. This detection limit was substantially lower than those of the previously reported colorimetric sensors for organophosphorus pesticides (Table S1), including those based on other nanozyme systems such as Fe–Mn dual-single-atom catalysts, MnO_2 nanosheets, and Ag nanoparticles. The superior sensitivity could be attributed to the signal amplification inherent in the enzymatic TCl generation coupled with the high catalytic efficiency of intact Cu-BTC, as well as the low background signal achieved through effective MOF disintegration in inhibitor-free samples. This strategy can be readily extended to the detection of other AChE inhibitors, demonstrating its broad applicability.

3.6. Stability, reproducibility, and interference study of the assay

The operational stability of the proposed colorimetric sensing system was evaluated over eight consecutive assay cycles. In each cycle, the absorbance of oxTMB was measured at 652 nm in a 0.1 M NaAc–HAc buffer (pH 4.5) following treatment with the chlorpyrifos solution (1.0×10^{-7} M). As illustrated in Fig. 5a, the UV–vis absorption at 652 nm remained stable throughout the testing period, yielding a calculated relative standard deviation (RSD) of 1.78%, indicating satisfactory operational stability. The reproducibility of the colorimetric sensor was examined by preparing six independent sensors toward 1.0×10^{-7} M chlorpyrifos. As depicted in Fig. 5b, the resulting absorbance values exhibited an RSD of 1.63%, confirming that the colorimetric sensing system possessed acceptable reproducibility.

To evaluate the selectivity of the sensor, common interferents that usually coexist with chlorpyrifos were examined. Potential interferents such as Fe^{3+}, Cu^{2+}, Mg^{2+}, and other pesticides were selected for the assessment. In all selectivity tests, the concentration of each interfering substance was 100 times that of chlorpyrifos. As depicted in Fig. 5c, significant signals were obtained only in the presence of the target analyte chlorpyrifos and its mixture, even at interfering concentrations 100-fold higher than that of chlorpyrifos. These findings demonstrated that the colorimetric method offered high selectivity and robust anti-interference capability for practical applications.

3.7. Determination of chlorpyrifos in real samples

To further validate the practical reliability of the biosensor, its performance was evaluated in apple samples spiked with

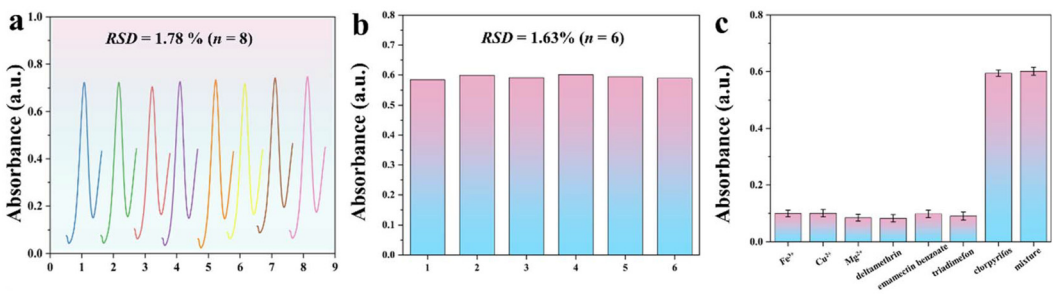

Fig. 5 (a) Stability test of the developed biosensor incubated with 10^{-7} M chlorpyrifos (n = 8). (b) Reproducibility of the biosensor incubated with 10^{-7} M chlorpyrifos (n = 6). (c) Interference study of chlorpyrifos using a 100-fold concentration of possible interferents.

chlorpyrifos at five concentration levels. The method yielded excellent recovery values ranging from 98.83% to 109.81% with an RSD of less than 2.57% (Table S2). These results indicate that the established sensor exhibits high accuracy and is suitable for reliable chlorpyrifos detection in real samples.

4. Conclusions

In summary, this study successfully developed a "turn-on" colorimetric sensor based on the instability of Cu-BTC nanozymes exhibiting peroxidase-like enzymatic activity, enabling the detection of AChE inhibitors. Cu-BTC has been proven to be unstable in the presence of S-containing molecules such as thiocholine. By leveraging this feature, the product of the AChE-catalyzed hydrolytic reaction induces the breakdown of Cu-BTC and further inhibits TMB oxidation. The proposed sensor allows for the rapid and sensitive quantification of chlorpyrifos in the concentration range of 10^{-4}–10^{-11} M with a visible color change at an LOD of 8.95 pM. This work not only illustrates an efficient strategy to construct sensors for –SH-containing molecules but also offers new insights into utilizing the instability of MOFs. Although Cu-BTC exhibits selective decomposition toward enzymatically generated thiocholine, potential interference from other biological thiols present in complex food matrices cannot be completely excluded. Such interferences might lead to false-positive signals in the analysis of real samples. Future work will focus on developing a dual-channel sensing platform, which could involve the incorporation of a reference probe or an internal standard that responds specifically to non-target thiols, enabling signal correction through ratiometric measurements.

Conflicts of interest

The authors declare no competing interests.

Data availability

The authors confirm that the data supporting the findings of this study are available within the article and its supplementary information (SI). Supplementary information is available. See DOI: https://doi.org/10.1039/d6an00156d.

Acknowledgements

The authors appreciate financial support from the Joint Project supported by the Natural Science Foundation of Science and Technology Department of Liaoning Province (2023-BSBA-294, 2023-BSBA-296, and 2024-MSLH-451) and the Basic Scientific Research Project for Universities of the Liaoning Education Department (LJ212510164028).

References

1 R. Kaur, D. Choudhary, S. Bali, S. S. Bandral, V. Singh, M. A. Ahmad, N. Rani, T. G. Singh and B. Chandrasekaran, Pesticides: an alarming detrimental to health and environment, *Sci. Total Environ.*, 2024, **915**, 170113.
2 R. Bi and G. Su, From target to unknown: comprehensive identification and risk assessment of organophosphate pesticides in foodstuffs, *J. Agric. Food Chem.*, 2025, **73**, 14058–14069.
3 Q. He, H. Su, H. Jiang, L. Liu and S. Zhang, Responsive release of guest aqueous droplet in liquid crystal droplet assists the detection of organophosphorus using commercial pregnancy test strip, *Sens. Actuators, B*, 2025, **423**, 136777.
4 X. Yuan, F. Wu, L. Cheng, T. Ji, C. Zheng, Y. Ma, Y. Jin, J. Dong, Y. Jin and B. Fang, Chlorpyrifos inhibits intestinal stem cell proliferation and differentiation at the acceptable daily intake and disrupts immune responses at high doses, *J. Agric. Food Chem.*, 2025, **73**, 12455–12464.
5 K. Niu, Y. Zhang, J. Chen and X. Lu, 2D conductive covalent organic frameworks with abundant carbonyl groups for electrochemical sensing, *ACS Sens.*, 2022, **7**, 3551–3559.
6 D. Du, S. Chen, J. Cai and A. Zhang, Immobilization of acetylcholinesterase on gold nanoparticles embedded in sol-gel film for amperometric detection of organophosphorus insecticide, *Biosens. Bioelectron.*, 2007, **23**, 130–134.
7 M. Brouwer, T. Koeman, P. A. van den Brandt, H. Kromhout, L. J. Schouten, S. Peters, A. Huss and R. Vermeulen, Occupational exposures and parkinson's disease mortality in a prospective dutch cohort, *Occup. Environ. Med.*, 2015, **72**, 448–455.
8 X. X. Kang, Ji. Yuan, X. J. Gu, X. Y. Li, T. Wen, M. He, Y. He, X. X. Yang, Y. C. Li, C. L. Guo, H. W. Ji, Y. L. Qin and L. Wu, DNA-Templated Ag nanocluster/CdSe@ZnS quantum dot-based platform for colorimetric and fluorescence detection of organophosphorus pesticide, *ACS Appl. Nano Mater.*, 2025, **8**, 1663–1672.
9 A. Arya, R. Chahal, R. Rao, M. H. Rahman, D. Kaushik, M. F. Akhtar, A. Saleem, S. M. A. Khalifa, H. R. El-Seedi, M. Kamel, G. M. Albadrani, M. M. Abdel-Daim and V. Mittal, Acetylcholinesterase inhibitory potential of various sesquiterpene analogues for alzheimer's disease therapy, *Biomolecules*, 2021, **11**, 350.
10 J. G. Zhou, Q. J. Tang, T. Wu and Z. H. Cheng, Improved TLC bioautographic assay for qualitative and quantitative estimation of tyrosinase inhibitors in natural products, *Phytochem. Anal.*, 2017, **28**, 115–124.
11 Y. P. Lai, S. H. He, Y. Y. Chen, T. R. Lin, L. Hou and S. L. Zhao, Hydrogen-bonded organic framework nanozyme with multi-enzyme activity for chemiluminescence sensing of acetylcholinesterase and screening its inhibitors, *Anal. Chem.*, 2025, **97**, 8362–8369.
12 M. L. Satnami, S. Ghosh, R. Nagwanshi, I. Karbhal, V. Jain, Y. Chawre, A. B. Kujur, A. Sinha, K. K. Ghosh, S. Pervez and

B. Gupta, Assessment of acetylcholinesterase activity using the gold nanocluster–MnO_2 nanosheet pair for detection of paraoxon, *ACS Appl. Nano Mater.*, 2024, **7**, 19657–19667.

13 Y. T. Cai, Y. Li, Y. Y. Wang, Y. H. Xu, T. Y. Chen, R. S. Xue, Y. M. Liu, W. Chen, X. R. Yang, Z. Liu, X. F. Bao and Z. Z. Huang, Triple-mode sensing platform for acetylcholinesterase activity monitoring and anti-Alzheimer's drug screening based on a highly stable Cu(I) compound, *Biosens. Bioelectron.*, 2025, **271**, 117078.

14 Q. Wu, Y. F. Wang, L. X. Wang, Y. Su, G. R. He, X. J. Chen, L. Hou, W. Y. Zhang and Y. Y. Wang, A portable electrochemical biosensor based on an amino-modified ionic metal–organic framework for the one-site detection of multiple organophosphorus Pesticides, *ACS Appl. Mater. Interfaces*, 2024, **16**, 55802–55812.

15 F. Zhang, Y. Gao, E. X. Ren, L. Fang, W. J. Yang, L. Y. Zhang and Z. W. Wang, Paper-based multicolor sensor for on-site quantitative detection of organophosphate pesticides based on acetylcholinesterase-mediated paper-based Au^{3+}-etching of gold nanobipyramids and CIELab color space, *Talanta*, 2025, **281**, 126925.

16 Y. Chawre, M. L. Satnami, A. B. Kujur, K. K. Ghosh, R. Nagwanshi, I. Karbhal, S. Pervez and M. K. Deb, Förster Resonance energy transfer between multicolor emissive N-Doped carbon quantum dots and gold nanorods for the detection of H_2O_2, glucose, glutathione, and acetylcholinesterase, *ACS Appl. Nano Mater.*, 2023, **6**, 8046–8058.

17 L. Liang, R. T. Yang, J. Wu, Y. Qin, Y. T. Jiang, S. L. Zhao and F. G. Ye, Analyte-induced specific regulation of light-responsive COF-Cu nanozyme activity for ultrafast thiram colorimetric sensing, *Anal. Chem.*, 2024, **96**, 18545–18554.

18 Q. Zhang, Z. G. Liu, Y. J. Han, Z. P. Li, L. F. Fan and Y. J. Guo, A colorimetric sensor based on cationic F-MOF/hemin-graphene peroxidase nanozymes for the detection of perfluorinated compounds, *Anal. Chem.*, 2025, **97**, 26108–26117.

19 Y. P. He, X. Z. Wang, C. Zhang, J. K. Sun, J. Z. Xu and D. F. Li, Near-Infrared light-mediated cyclodextrin metal–organic frameworks for synergistic antibacterial and antibiofilm therapies, *J. Am. Chem. Soc.*, 2023, **19**, 20232300199.

20 A. Chaouiki, M. Chafiq, R. Salghi, N. Elboughdiri, J. H. Kang, Y. G. Ko and M. Abboud, Versatile integration of MOF and MXene composites for next-generation hybrid energy storage solutions, *J. Energy Chem.*, 2025, **104**, 687–715.

21 N. Wang, J. J. Du, X. Li, X. L. Ji, Y. L. Wu and Z. L. Sun, Magnetic MOF substrates for the rapid and sensitive surface-enhanced raman scattering detection of uranyl, *Anal. Chem.*, 2023, **95**, 12956–12963.

22 T. Lian, R. Peng, Z. Y. Xiao, X. M. Tang, P. Xu, Y. Hu and P. Qiu, MOF-on-MOF nanomaterial (Fe-MOF@UiO-66)-based radiometric fluorescence/colorimetric dual-mode sensor for ultrasensitive detection of uric acid, *Anal. Chim. Acta*, 2025, **22**, 1368344325.

23 I. Senkovska, V. Bon, A. Mosberger, Y. T. Wang and S. Kaskel, Adsorption and separation by flexible MOFs, *Adv. Mater.*, 2025, **37**, 2414724.

24 Y. Chen, Y. Wang, C. Y. Yang, S. Wang, J. F. Yang and J. P. Li, Antenna-Protected metal–organic squares for water/ammonia uptake with excellent stability and regenerability, *ACS Sustainable Chem. Eng.*, 2017, **5**, 5082–5089.

25 X. L. Lv, S. Yuan, L. H. Xie, H. F. Darke, Y. Chen, T. He, C. Dong, B. Wang, Y. Z. Zhang, J. R. Li and H. C. Zhou, Ligand-rigidification for enhancing the stability of metal–organic frameworks, *J. Am. Chem. Soc.*, 2019, **141**, 10283–10293.

26 L. J. Wang, X. T. Li, B. Yang, K. Xiao, H. B. Duan and H. Z. Zhao, The chemical stability of metal-organic frameworks in water treatments: Fundamentals, effect of water matrix and judging methods, *Chem. Eng. J.*, 2022, **450**, 138215.

27 C. Xiao, J. D. Tian, Q. H. Chen and M. C. Hong, Water-stable metal–organic frameworks (MOFs): rational construction and carbon dioxide capture, *Chem. Sci.*, 2024, **15**, 1570–1610.

28 S. B. Luo, N. P. Deng, H. Wang, Q. Zeng, Y. N. Li, W. M. Kang and B. W. Cheng, Facilitating Li^+ conduction channels and suppressing lithium dendrites by introducing Zn-based MOFs in composite electrolyte membrane with excellent thermal stability for solid-state lithium metal batteries, *Chem. Eng. J.*, 2023, **474**, 145683.

29 Y. Li, B. L. Chai, H. Xu, T. F. Zheng, J. L. Chen, S. J. Liu and H. R. Wen, Temperature and solvent-induced reversible single-crystal-to-single-crystal transformations of TbIII-based MOFs with excellent stabilities and fluorescence sensing properties toward drug molecules, *Inorg. Chem. Front.*, 2022, **9**, 1504–1513.

30 X. Y. Sun, H. J. Zhang, X. Y. Zhao, Q. Sun, Y. Y. Wang and E. Q. Gao, Dual functions of pH-sensitive cation Zr-MOF for 5-Fu: large drug-loading capacity and high-sensitivity fluorescence detection, *Dalton Trans.*, 2021, **50**, 10524–10532.

31 R. Huo, C. Wang, F. Xu, Y.-H. Xing, Y. F. Wang and F. Y. Bai, Multistimuli-responsive pyrene-based lanthanide (III)-MOF construction and applied as dual-function fluorescent chemosensors for trace water and vitamins molecules, *Mater. Today Chem.*, 2023, **27**, 101292.

32 W. J. Wang, W. W. Yang, M. Schliephake, T. H. Zhao, Y. Liu, N. Hussain, B. Breitung, A. H. Schäfer, P. A. Levkin, J. Aghassi-Hagmann, A. K. Powell and M. Hirtz, Multiplexed fluorescent microarrays on MIL-101(Cr) thin films as luminescent probes for pH and disease-associated molecules, *Small*, 2025, **21**, 04783.

33 X. Y. Li, X. Gao, P. P. Gai, X. J. Liu and F. Li, Degradable metal-organic framework/methylene blue composites-based homogeneous electrochemical strategy for pesticide assay, *Sens. Actuators, B*, 2020, **323**, 128701.

34 J. F. Chang, W. X. Lv, Q. Li, H. Y. Li and F. Li, One-step synthesis of methylene blue-encapsulated zeolitic imidazolate framework for dual-signal fluorescent and homogeneous electrochemical biosensing, *Anal. Chem.*, 2020, **92**, 8959–8964.

35 X. L. Gao, H. F. Zhao, X. D. Zhao, Z. J. Li, Z. Q. Gao, Y. Y. Wang and H. L. Huang, Aqueous phase sensing of

bismuth ion using fluorescent metal-organic framework, *Sens. Actuators, B*, 2018, **266**, 323–328.

36 J. Deng, K. Wang, M. Wang, P. Yu and L. Mao, Mitochondria targeted nanoscale zeolitic imidazole framework-90 for ATP imaging in live cells, *J. Am. Chem. Soc.*, 2017, **139**, 5877–5882.

37 X. Yang, Q. Tang, Y. Jiang, M. Zhang, M. Wang and L. Mao, Nanoscale ATP-responsive zeolitic imidazole framework-90 as a general platform for cytosolic protein delivery and genome editing, *J. Am. Chem. Soc.*, 2019, **141**, 3782–3786.

38 L. Zhang and Y. H. Hu, Strong effects of higher-valent cations on the structure of the zeolitic Zn(2-methylimidazole)$_2$ framework (ZIF-8), *J. Phys. Chem. C*, 2011, **115**, 7967–7971.

39 L. L. Lu, X. H. Hu, R. J. Zeng, Q. Y. Lin, X. Huang, M. J. Li and D. P. Tang, Dual-mode colorimetric-photothermal sensing platform of acetylcholinesterase activity based on the peroxidase-like activity of Fe-N-C nanozyme, *Anal. Chim. Acta*, 2022, **1229**, 340383.

40 J. W. Liu, W. H. Wang, S. Y. Zhang, J. T. Jiang, M. W. He, W. L. Chen, Y. S. Gao, L. B. Deng, Q. Zhang, S. W. Liu, L. Y. Wang and L. M. Lu, COF encapsulated bio-enzyme cascade Fe/Cu-MOF nanozyme to strengthen environmental tolerance of electrochemical/colorimetric dual-modal sensor toward pesticide residue monitoring, *Sens. Actuators, B*, 2026, **448**, 139028.

41 X. D. Zhao, Y. Z. Zhang, J. M. Han, H. M. Jing, Z. Q. Gao, H. L. Huang, Y. Y. Wang and C. L. Zhong, Design of "turn-on" fluorescence sensor for L-Cysteine based on the instability of metal-organic frameworks, *Microporous Mesoporous Mater.*, 2018, **268**(15), 88–92.

42 F. Ke, L. G. Qiu, Y. P. Yuan, F. M. Peng, X. Jiang, A. J. Xie, Y. H. Shen and J. F. Zhu, Thiol-functionalization of metal-organic framework by a facile coordination-based postsynthetic strategy and enhanced removal of Hg^{2+} from water, *J. Hazard. Mater.*, 2011, **196**, 36–43.

43 J. Ethiraj, F. Bonino, C. Lamberti and S. Bordiga, H_2S interaction with HKUST-1 and ZIF-8 MOFs: A multitechnique study, *Microporous Mesoporous Mater.*, 2015, **207**, 90–94.

44 H. L. Tan, Q. Li, Z. C. Zhou, C. J. Ma, Y. H. Song, F. G. Xu and L. Wang, A sensitive fluorescent assay for thiamine based on metal-organic frameworks with intrinsic peroxidase-like activity, *Anal. Chim. Acta*, 2015, **856**, 90–95.